Pre-scission neutron multiplicity associated with the dynamical process in superheavy mass region

Yoshihiro Aritomo[1], Masahisa Ohta[2] and Francis Hanappe[3]

[1] Flerov Laboratory of Nuclear Reactions, JINR, Dubna, Russia
[2] Department of Physics, Konan University, 8-9-1 Okamoto, Kobe, Japan
[3] Universite Libre de Bruxelles, 1050 Bruxelles, Belgium

E-mail: aritomo24@muj.biglobe.ne.jp

Abstract. The fusion-fission process accompanied by neutron emission is studied in the superheavy-mass region on the basis of the fluctuation-dissipation model combined with a statistical model. The calculation of the trajectory or the shape evolution in the deformation space of the nucleus with neutron emission is performed. Each process (quasi-fission, fusion-fission, and deep quasi-fission processes) has a characteristic travelling time from the point of contact of colliding nuclei to the scission point. These dynamical aspects of the whole process are discussed in terms of the pre-scission neutron multiplicity, which depends on the time spent on each process. We have presented the details of the characteristics of our model calculation in the reactions ^{48}Ca+^{208}Pb and ^{48}Ca+^{244}Pu, and shown how the structure of the distribution of pre-scission neutron multiplicity depends on the incident energy.

1. Introduction

Recently, spectacular news on the finding of superheavy elements has been successively reported from FLNR, GSI and RIKEN [1, 2, 3, 4, 5, 6]. In theoretical approaches, the clarification of the reaction mechanism in the superheavy mass region and the prediction of the favorable conditions (projectile-target combination and beam energy values) to synthesize new elements have advanced step by step in the last few years [7, 8, 9, 10, 11, 12, 13]. However, we are still seeking suitable models for calculating the fusion and the survival probabilities, and investigating the unknown parameters involved in them. The fusion-fission mechanism in the superheavy-mass region must be elucidated; in particular, a more accurate estimation of fusion probability should be established.

Generally, on the base of analysis of the experimental mass, kinetic energy, and angular distributions of the reaction fragments, the whole reaction process in heavy nucleus collisions is classified into the fusion-fission, quasi-fission and deep inelastic collision processes and so on. Generally, mass symmetric fission fragments have been considered to originate from a compound nucleus. Therefore, in the experiment, the fusion-fission cross section has been derived by counting mass symmetric fission events [14].

However, in our previous work [15], we showed that it is ambiguous to identify mass symmetric fission events as the fusion-fission process in the superheavy-mass region. Using the Langevin equation, which enables to calculate the time development of a trajectory of a colliding system in a shape parameter space, we attempted to distinguish different dynamical paths by analyzing the trajectories and mass distribution of fission fragments. We identified the fusion-fission (FF) path, the quasi-fission (QF) path and the deep inelastic collision (DIC) path. In addition, in the reaction ^{48}Ca+^{244}Pu, we found a new path, called the deep quasi-fission (DQF) path, whose trajectory does not reach the spherical compound nucleus but goes to the mass symmetric fission area. The conclusion is that the analysis of only the mass distribution of fission fragments is insufficient to identify the reaction process described between the FF and DQF paths. To estimate the fusion probability accurately, the precise identification of the FF path is very important.

On the basis of experimental results, it has also been suggested that the reaction process may be classified by the measurement of the pre-scission neutron multiplicity, which correlates with the mass distribution of fission fragments [14, 16, 17]. This means that each process is expected to have its own characteristic reaction time, which is related to the pre-scission neutron multiplicity.

Hence, to identify the reaction process more precisely, we undertake to extend our model discussed in reference [15], by taking into account the effect of neutron emission along the dynamical path. We introduce the effect of neutron emission into the three-dimensional Langevin calculation code, or we combine the fluctuation and dissipation dynamical model with a statistical model. The preliminary analysis along this line has

been done in the reaction system ^{58}Ni+^{208}Pb at a incident energy corresponding to the excitation energy of the compound nucleus $E^* = 185.9$ MeV, which is a high incident energy case [18].

In this study, we have applied our model to the investigation of the whole dynamical process in the reactions ^{48}Ca+^{208}Pb and ^{48}Ca+^{244}Pu mainly at $E^* = 50$ MeV, that is to say, a low incident energy case. These reactions are chosen in order to precisely investigate the fusion process in the hot fusion reaction that has recently been performed at FLNR [19]. Also we discuss how the characteristic structure of the neutron multiplicity depends on the incident energy.

In section 2, we explain our framework for the model used here. We discuss the pre-scission neutron multiplicity with respect to fission fragments in section 3. The mechanism of the fusion-fission process with neutron emission is investigated. In section 4, we present a summary and further discussion.

2. Model

Using the same procedure as described in reference [15] to investigate the whole process dynamically, we use the fluctuation-dissipation model and employ the Langevin equation. We adopt the three-dimensional nuclear deformation space given by two-center parameterization [20, 21]. The three collective parameters involved in the Langevin equation are as follows: z_0 (distance between two potential centers), δ (deformation of fragments) and α (mass asymmetry of the colliding nuclei); $\alpha = (A_1 - A_2)/(A_1 + A_2)$, where A_1 and A_2 denote the mass numbers of the target and the projectile, respectively. We assume that each fragment has the same deformations as the first approximation. In the present calculation, the neck parameter ϵ is fixed to be 1.0, so as to retain the contact-like configuration more realistically for two-nucleus collision. The definitions of the δ and ϵ are mentioned in reference [20, 21, 22].

The multidimensional Langevin equation is given as

$$\begin{aligned} \frac{dq_i}{dt} &= \left(m^{-1}\right)_{ij} p_j, \\ \frac{dp_i}{dt} &= -\frac{\partial V}{dq_i} - \frac{1}{2}\frac{\partial}{\partial q_i}\left(m^{-1}\right)_{jk} p_j p_k - \gamma_{ij}\left(m^{-1}\right)_{jk} p_k + g_{ij} R_j(t), \end{aligned} \tag{1}$$

where a summation over repeated indices is assumed. q_i denotes the deformation coordinate specified by z_0, δ and α. p_i is the conjugate momentum of q_i. V is the potential energy, and m_{ij} and γ_{ij} are the shape-dependent collective inertia parameter and dissipation tensor, respectively. A hydrodynamical inertia tensor is adopted in the Werner-Wheeler approximation for the velocity field, and the wall-and-window one-body dissipation is adopted for the dissipation tensor [23, 24, 25]. The detail is explained in reference [15].

The intrinsic energy of the composite system E_{int} is calculated for each trajectory as

$$E_{int} = E^* - \frac{1}{2}\left(m^{-1}\right)_{ij} p_i p_j - V(q, l, T), \tag{2}$$

where E^* denotes the excitation energy of the compound nucleus, and is given by $E^* = E_{cm} - Q$ with Q and E_{cm} denoting the $Q-$value of the reaction and the incident energy in the center-of-mass frame, respectively.

We take into account neutron emission in the Langevin calculation during the reaction process. The emission of neutrons which is calculated by the statistical model has been coupled to the three-dimensional Langevin equation. The proceeder is explained precisely in reference [18].

3. Reaction process and pre-scission neutron multiplicity

Our model is applied to the reaction systems ^{48}Ca+^{208}Pb and ^{48}Ca+^{244}Pu with the incident energy corresponding to the excitation energy of the compound nucleus, E^*=50 MeV. In our previous work [15], we have shown that our model calculations for the mass distribution of fission fragments agree well with the experimental data and also the fusion-fission cross section. On the basis of the results given in reference [15], we want to make a new trial to clarify the relationship between the dynamical process and the pre-scission neutron multiplicity, and to investigate whether the relation can be seen at E^*=50 MeV. These reactions are chosen bearing in mind the more precise estimation of the fusion probability in the so-called hot fusion reaction performed at FLNR in experiments on superheavy element synthesis [19].

In the preliminary investigation in reference [18], for the purpose of checking the applicability of our model, we have analyzed to the recent experiment, in which the pre-scission neutron multiplicity correlated with the mass distribution of fission fragments has been measured in the reaction ^{58}Ni+^{208}Pb at the incident energy corresponding to the excitation energy of compound nucleus $E^* = 185.9$ MeV. This experiment was done by DéMoN group [16]. Our model calculation has reproduced the characteristic trend of the experimental distribution of pre-scission neutron multiplicity, and distinguished the FF and QF processes among the mass symmetric fission events.

Also we have showed our preliminary results on this study in references [17, 26, 27, 28]. We investigated the neutron multiplicity in the reaction ^{48}Ca+^{244}Pu at E^*=40 MeV. The experiment of neutron multiplicity shows the two peaks near 2 and 4 neutron emission [17]. Such two peaks are originated by two different fusion-fission mechanism. It looks that the first peak comes from QF process and the second one comes from mainly DQF or FF. However, the calculation could not reproduce the two peaks [28]. Due to a low excitation energy, the lifetime of neutron emission is rather short. It is comparable to the time scale of the fluctuation of the trajectory. So we can not distinguish QF and DQF process clearly. Moreover the number of events of FF process is quit small at a low incident energy. The statistics of each event are not enough to analyze the process.

Here, we investigate further by applying in the reaction ^{48}Ca+^{208}Pb and ^{48}Ca+^{244}Pu, more precisely, with increasing the excitation energy $E^* = 50$ MeV. To discuss the dynamical process, we mainly focus on zero angular momentum case. For each angular momentum, the potential landscape changes but the mechanism of the

process essentially does not change [22].

3.1. Reaction $^{48}Ca+^{208}Pb$

Using the model presented in Sect.2, we calculate the pre-scission neutron multiplicity emitted from the reaction system ^{48}Ca+^{208}Pb at $E^* = 50$ MeV for angular momentum $l = 0$. In this system, the FF process is dominant, that is to say, the mass symmetric fission events are dominant.

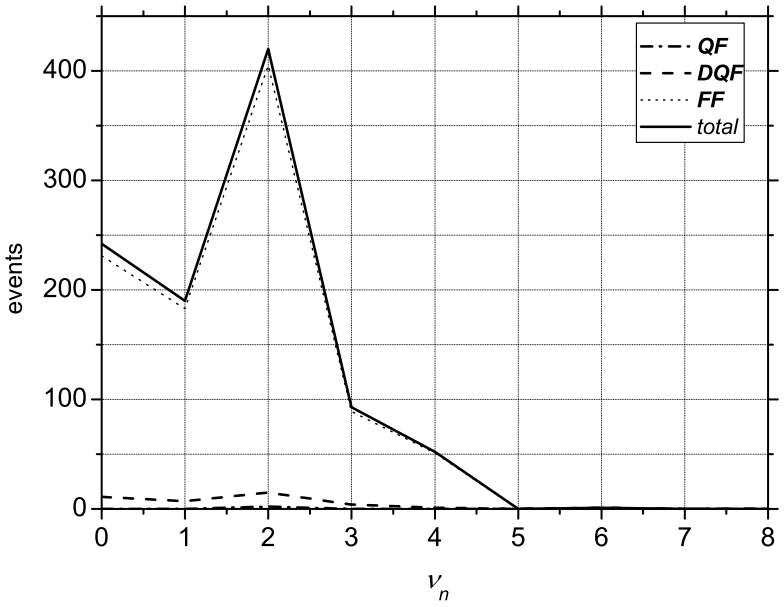

Figure 1. Pre-scission neutron multiplicities given by our theoretical calculation in the reaction ^{48}Ca+^{208}Pb at E^*=50 MeV for $l = 0$. The neutron multiplicity from the QF, DQF and FF processes are denoted by the dashed-dotted, the dashed and the dotted lines, respectively. The solid line denotes the total process.

The calculation is done in the same procedure as reference [22, 18]. In the three-dimensional Langevin calculation, we prepare 1,000 trajectories for each case. At $t = 0$, each trajectory starts from the point of contact. We define the fusion box as the region inside the fission saddle point, $\{z < 0.8, \delta < 0.3, |\alpha| < 0.3\}$ [15]. Samples of the trajectory of the FF process projected onto $z - \alpha$ ($\delta = 0$) plane in the reaction ^{48}Ca+^{208}Pb at $E^* = 50$ MeV for $l = 0$ is shown in Fig. 1 in reference [22]. The FF trajectory makes up 96% of all trajectories, and 95% of the FF trajectory escapes from the spherical region within 5.0×10^{-19} sec.

Figure 1 shows the distribution of the pre-scission neutron multiplicity ν_n in this reaction. The multiplicities from the QF, DQF and FF processes are denoted by the dashed-dotted line, dashed line and dotted line, respectively. The solid line shows the total multiplicity of each process. The distribution of pre-scission neutron multiplicity

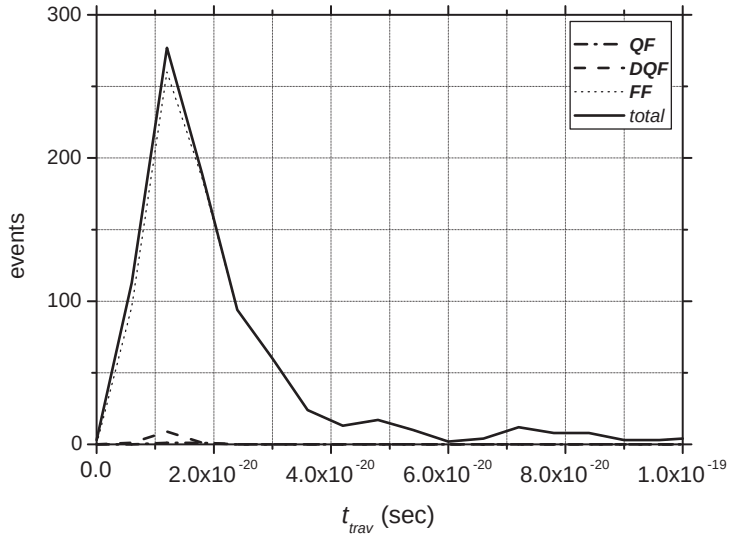

Figure 2. The distribution of travelling time t_{trav} in the reaction ^{48}Ca+^{208}Pb at $E^* = 50$ MeV for $l = 0$. The t_{trav} from the QF, DQF and FF processes are denoted by the dashed-dotted line, dashed line and dotted line, respectively. The solid line denotes the total process.

has a peak around $\nu_n = 2$. Since the FF process is dominant, the peak corresponds to the FF process.

We define the travelling time t_{trav} as a time duration during which the trajectory moves from the point of contact to the scission point. We present the distribution of the travelling times for the QF, DQF and FF processes in Fig. 2, denoted by the dashed-dotted line, dashed line and dotted line, respectively. The solid line shows the distribution of the travelling time for all processes. In the FF process, as discussed in reference [22], the trajectory is trapped in the pocket around the spherical region. Consequently, the trajectory spends a relatively long time in the pocket before it finally escapes from there. The travelling time of the FF process has a peak at 1.2×10^{-20} sec, and the average time of it is 15.3×10^{-20} sec.

As shown in reference [18], in the reaction system ^{58}Ni+^{208}Pb at $E^* = 185.9$ MeV, the distribution of the neutron multiplicity has two peaks which come from the QF and FF processes, respectively. On the other hand, Fig. 1 shows the single peak.

For the ^{48}Ca+^{208}Pb reaction, the FF process is dominant in this energy region, in consistent with the potential energy surface shown in Fig. 1 in reference [22], in which we can see the steep valley in the entrance mass asymmetry and in the mass symmetric fission valley. This fact is consistent with the pre-scission neutron multiplicity having only a single peak at ν_n=2, which indicates that only one process is dominant.

In the preliminary calculation [28], we have compared the results with the experimental data at $E^* = 40$ MeV [17], which shows the distribution of the pre-scission

neutron multiplicity in correlation with fission fragments whose mass number is grater than $\frac{A_{CN}}{2} - 30$ and less than $\frac{A_{CN}}{2} + 30$, where A_{CN} denotes the mass number of the compound nucleus. The tendency of these results coincides with the experimental data.

3.2. Reaction ^{48}Ca+^{244}Pu

In reference [15, 22], the whole dynamical process in the reaction ^{48}Ca+^{244}Pu was classified into the QF, DQF and FF processes. At a low incident energy, the mass asymmetric fission events are dominant, which is the QF process [14]. We have distinguished between the DQF and the FF process by analyzing whether the trajectory enters the fusion box or not. The analysis only of the mass distribution for fission fragments is insufficient to distinguish between the DQF and the FF processes [15]. In the present study, we show how each process corresponds to a characteristic number of pre-scission neutron multiplicities at $E^* = 50$ MeV.

Samples of the trajectory of the QF, DQF and FF process projected onto $z - \alpha$ ($\delta = 0$) and $z - \delta$ ($\alpha = 0$) plane at $E^* = 50$ MeV for $l = 0$ in the reaction ^{48}Ca+^{242}Pu are shown in Fig. 5 in reference [22]. We define the fusion box as the region inside the fission saddle point, $\{z < 0.6, \delta < 0.2, |\alpha| < 0.25\}$ [15].

3.2.1. Classification on the basis of mass distribution of the fission fragments

Generally, it is considered that the reaction process is classified according to the mass distribution of fission fragments and their total kinetic energy distribution [14]. The QF process is defined as the fission fragments having mass number greater than $\frac{A_{CN}}{2} + 20$ and less than $\frac{A_{CN}}{2} - 20$. This condition is also suited to the deep inelastic collision process (DIC) in the present case. The FF process is defined by the condition that the trajectory enters the fusion box. The DQF process produces the mass symmetric fission fragments (greater than $\frac{A_{CN}}{2} - 20$ and less than $\frac{A_{CN}}{2} + 20$), but the system does not reach the spherical compound nucleus before undergoing fission. We name this method of classification as the "classification by fission fragments mass" (standard classification).

As discussed in reference [15], we can not distinguish between the FF and the DQF processes only using the fission fragment mass. The difference of the both processes is the reaction time, that is to say, the travelling time t_{trav}. We suppose that the neutron multiplicity depends on the t_{trav}. Here, we try to investigate the correlation between the neutron multiplicity and each process which is separated by using the standard classification.

As the result analizing 10,000 trajectories, it is found that the QF process (including a part of DIC), the DQF process and the FF process account for 72%, 25% and 3%, respectively. In Fig. 3, the neutron multiplicity from the QF, DQF and FF processes are denoted by the dashed-dotted line, solid line and gray line, respectively. The dashed line denotes the total multiplicity contributed from all processes.

Many trajectories go to the fission area without neutron emission. The travelling time of such a trajectory is rather short. As can be seen in Fig. 3, it is difficult to

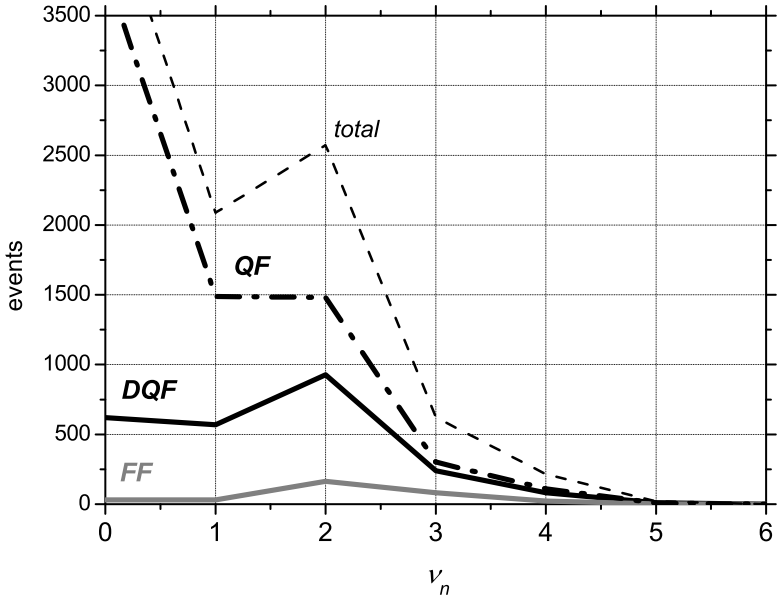

Figure 3. Pre-scission neutron multiplicity given by our theoretical calculation in the reaction ^{48}Ca+^{244}Pu at E^*=50 MeV for $l = 0$ with the classification method of using the mass distribution of fission fragments. The neutron multiplicity from the QF, DQF and FF processes are denoted the dashed-dotted, the solid and the gray lines, respectively. The dashed line denotes the total multiplicity of each process.

see a characteristic structure of the neutron multiplicity corresponding to the process classified. The total number of events for $2n$ emission is significant, but the QF and the DQF processes account for approximately equal contributions. These results show that there is no correlation between the neutron multiplicity and the mass distribution of the fission fragments in this incident energy.

Figure 4 shows the mass distribution of fission fragments for each process. The fission fragments from the QF+DIC, DQF and FF processes are presented by the light gray, the gray and the black shading, respectively. The thin black line denotes the total number of events of all processes. The fission fragments from the FF process spread from $A = 100$ to 200. Therefore, we can see that the FF process is related to both the mass symmetric fission and the mass asymmetric fission. In Fig. 4, two sharp peaks are located at $A \sim 80$ and $A \sim 210$. These events come from the trajectories that go down quickly along the valley at $\alpha \sim 0.42$ in the potential energy surface, which is the result of the the shell structure of the Pb nucleus.

The corresponding travelling times for each process are shown in Fig. 5. The peak of travelling time for the QF process, which is located at $t_{trav} \sim 7.5\times10^{-21}$ sec, is slightly shorter than the time at the peak of the DQF process. Until $t_{trav} = 3.0 \times 10^{-20}$ sec, the travelling time of DQF process overlaps with that of the QF process. The average travelling times of the QF, DQF and FF processes are $1.11, 1.73$ and 4.83×10^{-20} sec,

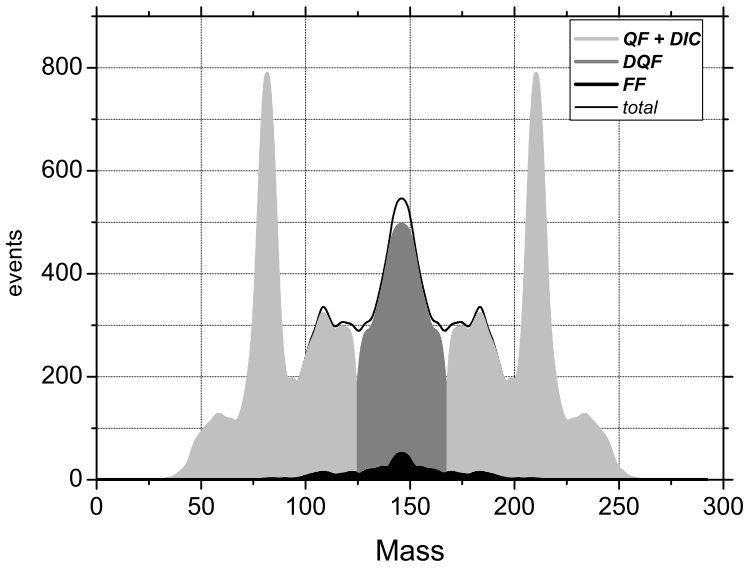

Figure 4. Mass distribution of fission fragments in the reaction ^{48}Ca+^{244}Pu at $E^* = 50$ MeV for $l = 0$ using the method of classification by fission fragment mass. The fission fragments from the QF+DIC, DQF and FF processes are presented by the light gray, the gray and the black shading, respectively. The thin black line denotes the total number of events of all processes.

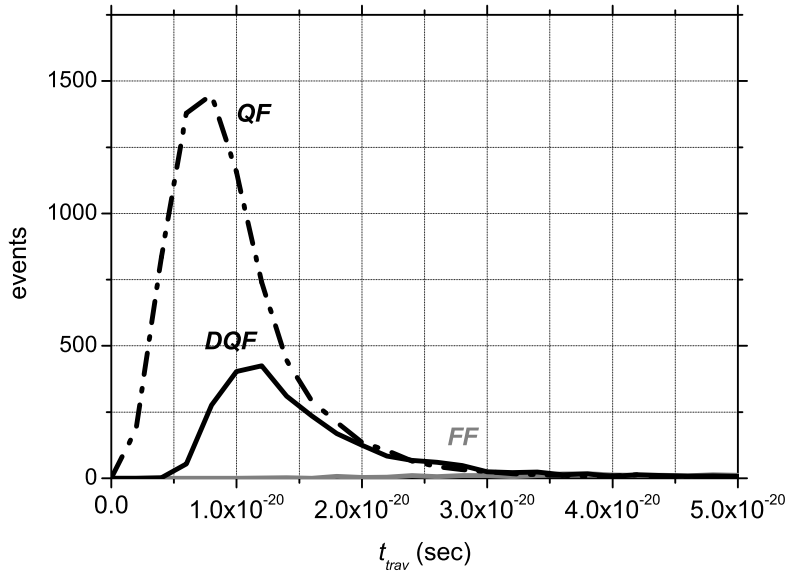

Figure 5. The distribution of the travelling time t_{trav} of each path in the reaction ^{48}Ca+^{244}Pu at $E^* = 50$ MeV for $l = 0$, using the method of classification by fission fragment mass.

respectively. The travelling time of the FF process is about three times as long as those of the QF and DQF processes.

3.2.2. Correlation between the travelling time t_{trav} and the neutron multiplicity ν_n
In the standard classification, we can not distinguish a characteristic structure of the neutron multiplicity corresponding to each process, in this low incident energy case. Here, we investigate the reason why the neutron multiplicity do not show the characteristic structure corresponding to the reaction process like as a high incident energy case [18]. In conclusion, the cause of this failure is the use of the fission fragment mass for the classification of processes. We discuss this point in this subsection.

As we discussed above, we expect that each process may have the characteristic reaction time. Here, at first we show the relation between the average travelling time $\langle t_{trav} \rangle$ and the mass number of the fission fragments in Fig. 6. The average travelling time of the mass symmetric fission process is longer than that of the mass asymmetric fission process. We can see clearly the correlation between the $\langle t_{trav} \rangle$ and the mass number of the fission fragments. The average travelling time for $\frac{A_{CN}}{2} - 20 < A < \frac{A_{CN}}{2} + 20$ is ranging from $1.8{\times}10^{-20}$ to $2.1{\times}10^{-20}$ sec. In Fig. 5, the fluctuations of the travelling time of the QF and the DQF processes, which are expressed by the distributions of the travelling time around the most probable value for each process, are ranging in the width of $2.5 \sim 3.0 \times 10^{-20}$ sec. These fluctuations of the travelling time are larger than the difference between the average travelling time of the QF and the DQF processes. Therefore, it is difficult to separate the QF and DQF processes by the travelling time.

The relation between the travelling time and each neutron multiplicity in this system is shown in Fig. 7. With increasing the time duration, the large neutron multiplicity is expected. At this incident energy, the events for $1n$ and $2n$ emission are dominant, and it corresponds to the peaks for the QF and DQF processes in Fig. 3. Due to the stochastic fluctuation in the statistical model, the time taking for the events of $1n$ and $2n$ emission are overlapped significantly. We can not distinguish the reaction time of the both processes by the number of neutron multiplicity.

The life time of the neutron emission and the travelling time are partly governed by the random number in the stochastic aspect which is contained in statistical model and the Langevin equation. The width of these fluctuation in time space is overlapped for each process in this case. Actually, at $E^* = 50$ MeV, the maximum number of evaporated neutron ν_n^{max} is approximately $4 \sim 5$ as shown in Fig. 3. However, as shown in Fig. 7, peaks for the different neutron multiplicity are not well separated so as to identify the reaction process. As we will show later, it is coming from small $\nu_n^{max} (\sim 4)$.

Figure 8 shows the neutron multiplicity associated with the mass number of fission fragments in the reaction ^{48}Ca+^{244}Pu at $E^* = 50$ MeV for $l = 0$. The two sharp peaks of $0n$ and $1n$ at $A = 80$ and 210 are caused by the trajectory which goes down along the valley near the Pb nucleus (or the Kr nucleus) in the potential energy surface. Such a trajectory quickly goes down to the fission area, so that it does not have large chance to emit any neutron. As can be seen in Fig. 8, there exist trajectories with a variety of

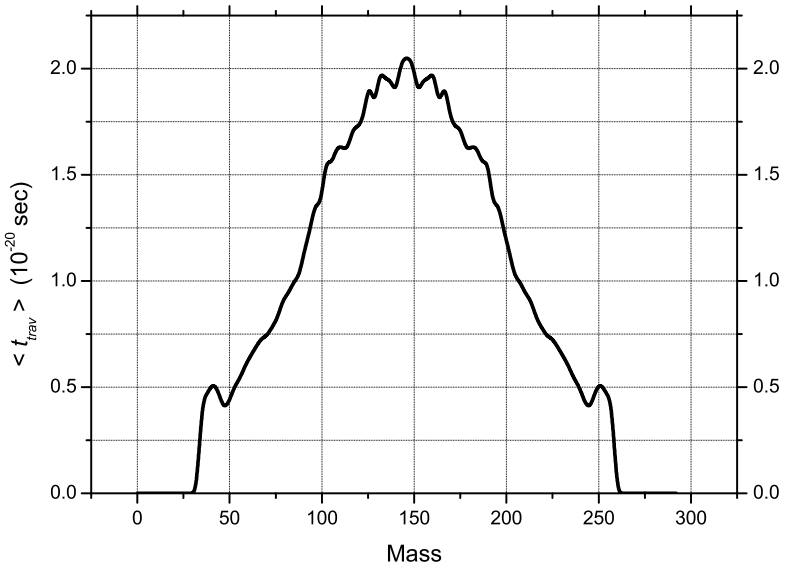

Figure 6. The average travelling time associated with fission fragment in the reaction ^{48}Ca+^{244}Pu at $E^* = 50$ MeV for $l = 0$.

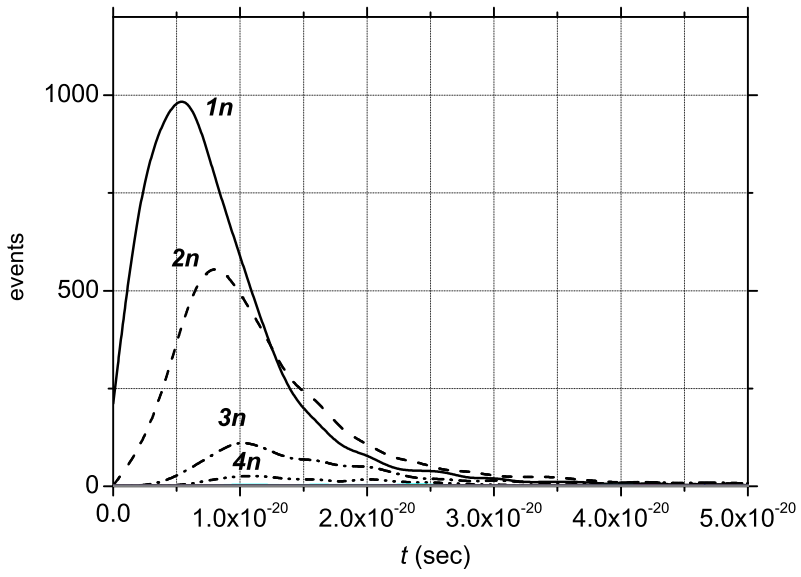

Figure 7. Time dependence of neutron multiplicity in the reaction ^{48}Ca+^{244}Pu at $E^* = 50$ MeV for $l = 0$. The neutron multiplicity are given.

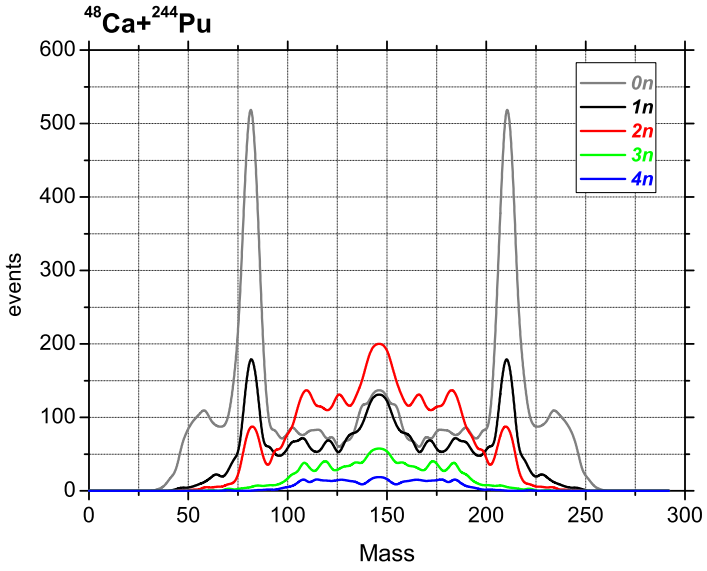

Figure 8. The neutron multiplicity associated with fission fragment in the reaction ^{48}Ca+^{244}Pu at $E^* = 50$ MeV for $l = 0$.

numbers of the neutron emission in the region $90 < A < 210$. The trajectories having different neutron multiplicities coexist in this region. With decreasing mass asymmetry, $2n$ and $3n$ events increase because, in this region, the number of trajectories with long travelling time increases as shown in Fig. 6.

The characteristic feature observed in Fig. 8 is that each neutron multiplicity spreads over a wide mass region of fission fragments. It is noteworthy that the events with even $0n$ and $1n$ are found in the mass symmetric fission area. Therefore, it is clear that we can not extract the characteristic structure of neutron multiplicity by means of the standard classification.

3.2.3. Classification using the additional condition on z As discussed in the previous subsection, the trajectories of each process spread over a wide mass region of fission fragments. We understand that each process has characteristic behavior. However, the information of the mass number of fission fragments does not clearly connected with the dynamical aspect of each process which we imaged. We have to look for the proper classification method that corresponds to our recognition of each process, instead of the method using fission fragment mass. Here, we propose to employ a classification method based on the dynamical trajectory of the process.

As shown in Fig. 3, the QF process includes the events of $4n$ emission. Such events account for about 1.5% of the total QF process. Generally, the QF process is regarded as a short process that does not have enough time to relax the degree of mass asymmetry. It may be unreasonable to consider that the QF process has sufficient time to evaporate

4 neutrons.

It is found that among the QF process some trajectories associated with 4 neutrons emission enter the region of small z and their travelling times seem longer than that of the typical sample trajectory presented in our previous paper [22]. These trajectories pass the scission points where the mass number is greater than $\frac{A_{CN}}{2} + 20$ ($\alpha = 0.136$) and less than $\frac{A_{CN}}{2} - 20$ ($\alpha = -0.136$), which is classified into the QF process by the standard classification. In particular, it is found that the mass asymmetry of such trajectory changes from $\alpha = 0.67$ to -0.3 in the region of small z. This QF process should be distinguished from the usual QF process.

We usually consider the trajectory of the DQF process to enter the small z region, but due to the strong Coulomb repulsion, it goes to the large-deformation region and returns to the fission area without passing the fusion box. Thus, considering this scenario, we add a condition to the standard classification discussed in the previous subsection.

Therefore, we define a new rule that a trajectory which enters the region of $z < 0.4$, where the nuclear shape resembles mono-nucleus, is to be reclassified into the DQF process, even though the mass fragments lie in the asymmetric region ($A < \frac{A_{CN}}{2} - 20$ and $A > \frac{A_{CN}}{2} + 20$). That is to say, the DQF process is redefined as the process that the trajectory enters the region of $z < 0.4$ without passing the fusion box. Actually, the distribution of the travelling time of such a trajectory occupies the region of longer t_{trav} of the QF process. We call this classification "the classification of the fission fragment mass with an additional condition on z".

Here, we should consider the process that the trajectory goes to mass symmetric fission region, where the mass number is greater than $\frac{A_{CN}}{2} - 20$ and less than $\frac{A_{CN}}{2} + 20$, but the trajectory does not enter the region of $z < 0.4$. We name this process the mass symmetric quasi-fission process (MSQF). In this system, the trajectory of the MSQF process occupies 1.21 % of the all trajectories, and 4.55% of the mass symmetric fission events. We can say that the almost mass symmetric fission events come from the trajectory which enters the region of $z < 0.4$.

By this classification, the component of the last QF process, which has a long travelling time, is classified into the DQF process. Such a trajectory accounts for about 32% of the total QF process. Figure 9 shows the each neutron multiplicity distribution by the new classification, where each line has the same meaning as that in Fig. 3. We can see that the peak of the DQF process at $\nu_n = 2$ is higher and the number of events increases compared with that in Fig. 3. Figure 10 shows the distribution of t_{trav} for each process using this new classification. The the travelling time of the DQF process and the QF process separates more clearly than that shown in Fig. 5. After $t_{trav} = 1.2 \times 10^{-20}$ sec, the DQF process is dominant.

The mass distribution of fission fragments is shown in Fig. 11. The shading and lines have the same meanings as those in Fig. 4. We can see that the fission fragments from the DQF process exist in the region of mass number greater than $\frac{A_{CN}}{2} + 20$ ($A = 166$) and less than $\frac{A_{CN}}{2} - 20$ ($A = 126$). In the regions $166 < A < 200$ and $90 < A < 126$,

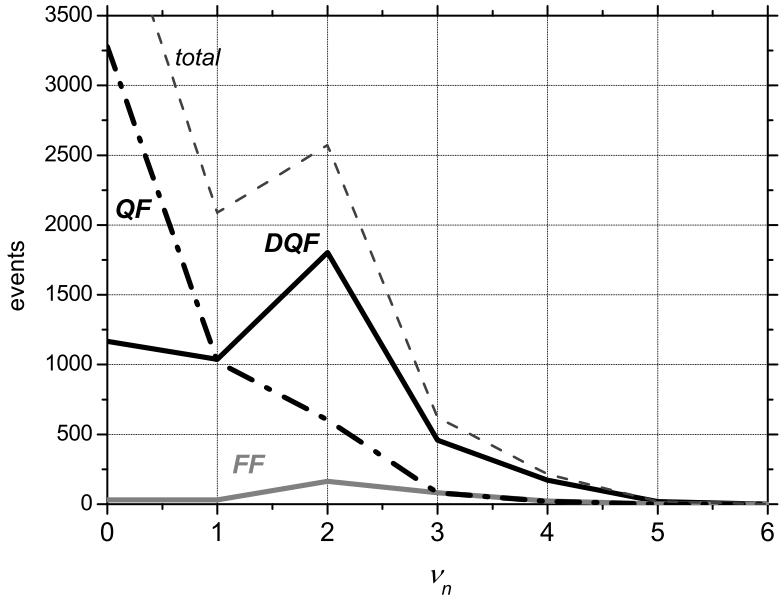

Figure 9. Pre-scission neutron multiplicity given by our theoretical calculation in the reaction ^{48}Ca+^{244}Pu at E^*=50 MeV for $l = 0$ using the method of classification by fission fragment mass adding a condition on z. The lines denote the same items as those in Fig. 3.

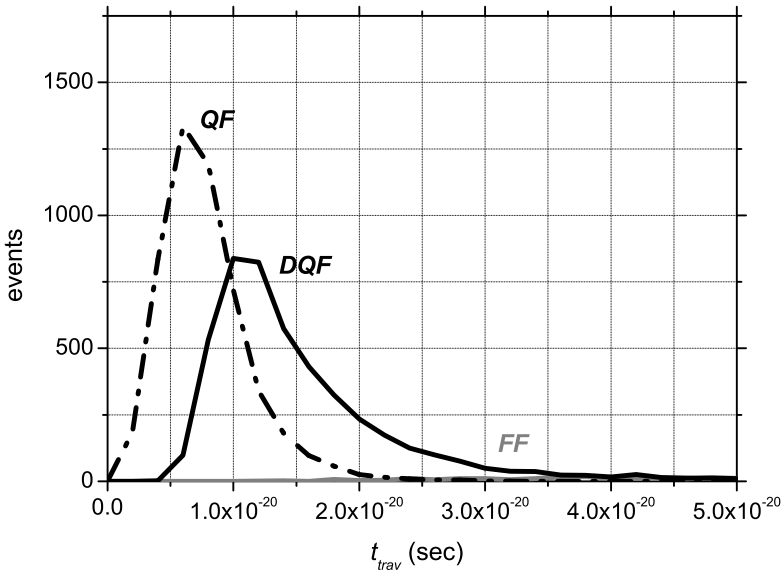

Figure 10. The distribution of the travelling time t_{trav} of each path in the reaction ^{48}Ca+^{244}Pu at $E^* = 50$ MeV for $l = 0$, using the method of classification by fission fragment mass adding a condition on z.

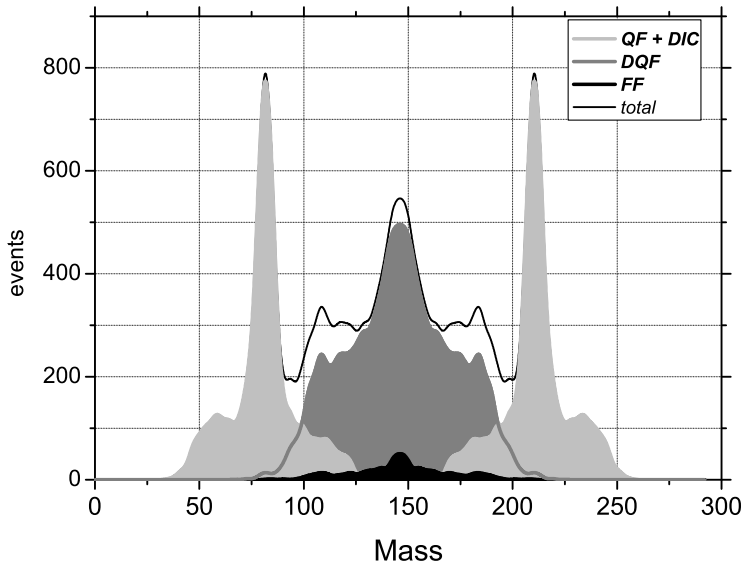

Figure 11. Mass distribution of fission fragments in the reaction ^{48}Ca+^{244}Pu at $E^* = 50$ MeV for $l = 0$ using the method of classification by fission fragment mass adding a condition on z. The shading and lines denote the same items as those in Fig. 4.

the DQF process and the QF process coexist. This means that the trajectories with long and short travelling times intermingle. That is to say, in this region, the fission fragment has two possible origins, one is the short process wherein the colliding partner goes quickly to the fission area, and the other is the long process in which the trajectory approaches the compact shape and takes a long time to arrive at the fission area.

3.2.4. Incident energy dependence in neutron multiplicity analysis As practice, in order to identify the details of the whole reaction process, we introduce the classification on the basis of trajectory's behavior by the theoretical calculation. When the experimental pre-scission neutron multiplicity is analyzed in combination with the trajectory calculation, the information on the neutron multiplicity can be put to practical use to clarify the reaction mechanism, that is to say we can distinguish the QF, DQF and FF processes.

At a high incident energy, the situation is different. When the incident energy increases, the distribution of the neutron multiplicity is spread well. The neutron multiplicity can become a good measure of each process [18, 26, 27, 28].

Figure 12 shows the distribution of the neutron multiplicity in the reaction ^{48}Ca+^{244}Pu at $E^* = 80$ MeV and $E^* = 160$ MeV for $l = 0$ in (a) and (b), respectively. Here, each line has the same meaning as that in Fig. 3. We use the classification of the fission fragment mass with an additional condition on z. With increasing the incident energy, the events of the QF process decrease because the mass symmetric fission events are dominant. The DQF and FF processes are well distinguished by the

neutron multiplicity at $E^* = 160$ MeV.

In the high incident energy case, ν_n^{max} increases, which are about 8 and 14 at $E^* = 80$ and 160 MeV, respectively. With increasing ν_n^{max}, it becomes possible to identify the reaction processes using the distribution of neutron multiplicity, because the neutron multiplicity spreads over the wide region and indicates the characteristic property of each process, which is not overlapped by the fluctuations.

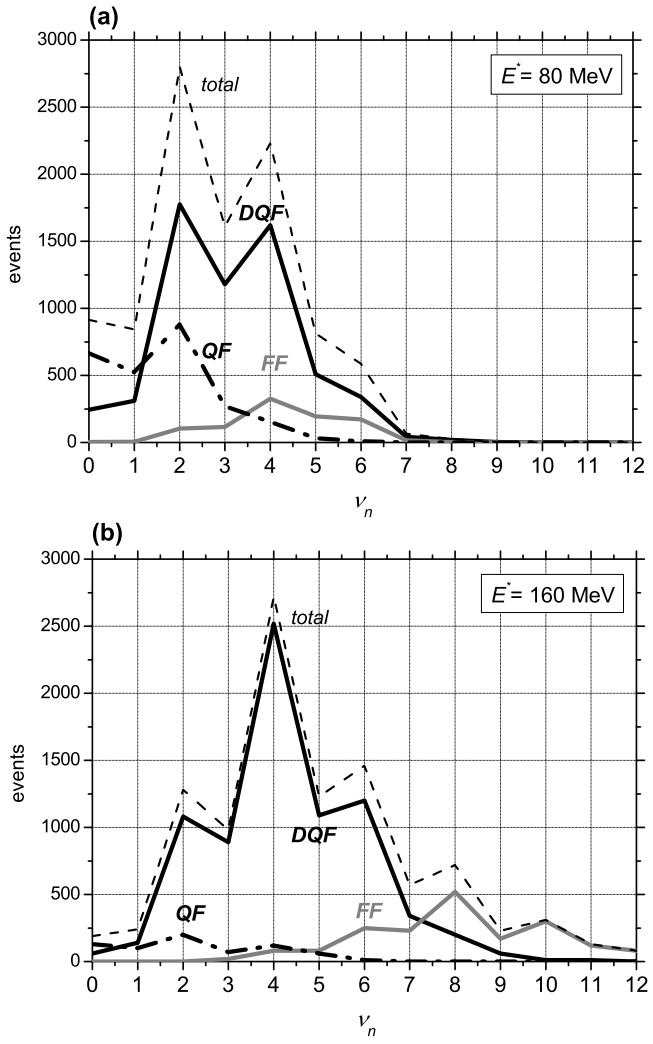

Figure 12. Pre-scission neutron multiplicity given by our theoretical calculation in the reaction ^{48}Ca+^{244}Pu at (a) E^*=80 MeV and (b) E^*=160 MeV for $l = 0$, using the method of classification by fission fragment mass adding a condition on z. The lines denote the same items as those in Fig. 3

Table 1 shows the average travelling time $\langle t_{trav} \rangle$ in the reaction ^{48}Ca+^{244}Pu for $l = 0$, using the classification method (i) the fission fragment mass (method (i)) and (ii) the fission fragment mass with additional condition on z (method (ii)). At $E^* = 50$

MeV, in method (i), the $\langle t_{trav} \rangle$ of the DQF process is about 1.5 times as long as that of the QF process. However, in method (ii), it is about twice as long. This is because the DQF process in method (ii) includes the long QF process in method (i). The $\langle t_{trav} \rangle$ of the DQF process in method (ii) does not change as much as that in method (i), because the long tail of the DQF process mainly influences the average time.

The $\langle t_{trav} \rangle$ at $E^* = 80$ MeV and 160 MeV are shown in Table 1, in the classification method (ii). We can see the incident energy dependence of $\langle t_{trav} \rangle$. With increasing the incident energy, the initial speed of the trajectory increases. After the kinetic energy dissipates, also the moving speed of trajectory by the fluctuation is high. As a result, $\langle t_{trav} \rangle$ becomes shorter. The ratio among the $\langle t_{trav} \rangle$ of QF, DQF and FF seems to be approximately constant for each incident energy.

Table 1. The average travelling time for each classification, in the reaction ^{48}Ca+^{244}Pu for $l = 0$. The methods of classification are based on (i) the fission fragment mass (method (i)) and (ii) the fission fragment mass with a condition on z (method (ii)).

	^{48}Ca+^{244}Pu			
	method (i)	method (ii)		
	$E^* = 50$ MeV	$E^* = 50$ MeV	$E^* = 80$ MeV	$E^* = 160$ MeV
	($\times 10^{-20}$sec)	($\times 10^{-20}$sec)	($\times 10^{-20}$sec)	($\times 10^{-20}$sec)
QF	1.11	0.88	0.85	0.73
DQF	1.73	1.69	1.58	1.38
FF	4.83	4.83	4.00	3.71

4. Summary

The fusion-fission process in the superheavy-mass region was studied on the basis of fluctuation-dissipation dynamics. In order to classify the reaction process in greater detail, we analyzed the pre-scission neutron multiplicity connecting with the mass distribution of fission fragments. The neutron multiplicity depends on the travelling time of the trajectory from the point of contact to the scission point. We introduced the effect of pre-scission neutron emission into the three-dimensional Langevin calculation, that is to say, we combined the Langevin code with the statistical code. We applied our model to the investigation of the whole reaction process in the reactions ^{48}Ca+^{208}Pb and

^{48}Ca+^{244}Pu at the incident energy corresponding to the excitation energy of a compound nucleus, $E^* = 50$ MeV.

In the reaction ^{48}Ca+^{208}Pb at $E^* = 50$ MeV, the reaction process is simple. Most of the process comprises the FF process. In this case, the pre-scission neutron multiplicity distribution shows a single peak at $\nu_n = 2$.

In the reaction ^{48}Ca+^{244}Pu at $E^* = 50$ MeV, the pre-scission neutron multiplicity distribution of the DQF process overlaps significantly with the distribution of the QF process, when we use the standard classification using only the information of mass distribution of fission fragments. Consequently, we could not distinguish between the QF and the DQF processes on the basis of the pre-scission neutron multiplicity. However, if we introduce the additional condition for the classification concerning with the travelling time of trajectories, we could show that the situation becomes to be resolved. The additional condition is that the trajectory entering into the area of $z < 0.4$ but not into the fusion box is classified to DQF process, even if the mass fragments distribute outside the region between $\frac{A_{CN}}{2} - 20$ and $\frac{A_{CN}}{2} + 20$. Using this classification, it was shown that the pre-scission neutron multiplicity distribution of the DQF process is clearly separated from that of the QF process.

We also discussed how the characteristic structure of the neutron multiplicity depends on the incident energy, and presented that we can get more and more clear structure corresponding to each reaction process when the incident energy increases.

In the next study, we would like to investigate parameters more precisely, for example, the friction tensor, the level density parameter and the neutron binding energy near di-nucleus configuration etc. We try to use the friction tensor which is derived from liner response theory at a low excitation energy [29, 30, 31].

Acknowledgement

The authors are grateful to Professor Yu. Ts. Oganessian, Professor M.G. Itkis, Professor V.I. Zagrebaev for their helpful suggestions and valuable discussion throughout the present work. The authors wish to thank Professor T. Wada who developed the original version of the calculation code for the three-dimensional Langevin equation. The special thanks are deserved to Dr. A.K. Nasirov for useful discussion. The authors thank Dr. S. Yamaji and his collaborators, who developed the calculation code for potential energy with a two-center parameterization. This work has been in part supported by INTAS projects 03-01-6417.

References

[1] Oganessian Yu Ts *et al* 1999 *Nature* **400** 242; Oganessian Yu Ts *et al* 1999 *Phys. Rev. Lett.* **83** 3154.
[2] Oganessian Yu Ts *et al* 2001 *Phys. Rev.* C **63** 011301(R).
[3] Oganessian Yu Ts *et al* 2004 *Phys. Rev.* C **69** 021601(R).

[4] Hofmann S and Münzenberg G 2000 *Rev. Mod. Phys.* **72** 73; Hofmann S *et al* 2002 *Eur. Phys. J* A **14** 147.
[5] Morita K*et al* 2004 *Nucl. Phys.* A **734** 101.
[6] Morita K*et al* 2004 *Journal of the Physical Society of Japan* **73** 2593.
[7] Zagrebaev V I and Greiner W 2005 *J. Phys.* G **31** 825
[8] Nasirov A, Fukushima A, Toyoshima Y, Aritomo Y, Muminov A, Kalandarov S and Utamuratov R 2005 *Nucl. Phys.* A **759** 342
[9] Diaz-Torres A and Scheid W 2005 *Nucl. Phys.* A **757** 373
[10] Świątecki W J, Siwek-Wilczyska K and Wilczyski J 2005 *Phys. Rev.* C **71** 014602
[11] Adamian G G and Antonenko N V 2005 *Phys. Rev.* C **72** 064617
[12] Mişicu Ş and Greiner W 2004 *Phys. Rev.* C **69** 054601
[13] Rummel C and Hofmann H 2003 *Nucl. Phys.* A **727** 24
[14] Itkis M G *et al* 2001 *Proc. Int. Conf. on Fusion Dynamics at the Extremes (Dubna)* ed Yu Ts Oganessian and V I Zagrebaev (Singapore: World Scientific) p.93.
[15] Aritomo Y and Ohta M 2004 *Nucl. Phys.* A **744** 3.
[16] Donadille L *et al* 1999 *Nucl. Phys.* A **656** 259.
[17] Materna T *et al* 2004 *Nucl. Phys* A **734** 184; Materna T *et al* 2004 *Prog. Theo. Phys.* **154** 442; Materna T *et al* 2004 *Int. Jour. Mod. Phys.* E **13** 258.
[18] Aritomo Y, Ohta M, Materna T, Hanappe F, Dorvaux O and Stuttgé L 2005 *Nucl. Phys.* A **759** 309.
[19] Oganessian Yu Ts *et al* 2004 *Phys. Rev.* C **69** 054607; Oganessian Yu Ts *et al* 2004 *Phys. Rev.* C **70** 064609.
[20] Mosel U, Maruhn J and Greiner W 1971 *Phys. Lett.* B **34** 587; Maruhn J and Greiner W 1972 *Z. Phys.* **251** 431.
[21] Sato K, Iwamoto A, Harada K, Yamaji S and Yoshida S 1978 *Z. Phys.* A **288** 383.
[22] Aritomo Y and Ohta M 2005 *Nucl. Phys.* A **A753** 152.
[23] Blocki J, Boneh Y, Nix J R, Randrup J, Robel M, Sierk A J and Swiatecki W J, 1978 *Ann. Phys.* **113** 330.
[24] Nix J R and Sierk A J 1984 *Nucl. Phys.* A **428** 161c.
[25] Feldmeier H 1987 *Rep. Prog. Phys.* **50** 915.
[26] Aritomo Y, Ohta M, Materna T, Hanappe F and Stutt'e L 2004 *Nucl. Phys.* A **734** 180.
[27] Aritomo Y, Ohta M, Materna T, Hanappe F and Stuttgé L 2004 *Structure and Dynamics of Elementary Matter*, ed Greiner W, Itkis M G, Reinhardt J and Guclu M C (Netherlands: Kluwer Academic Publishers) p.395.
[28] Aritomo Y, Ohta M, Materna T, Hanappe F and Stuttgé L 2004 *Nucl. Phys.* A **738** 221.
[29] H. Hofmann, Phys. Rev. **284** (1997), 137.
[30] S. Yamaji, F.A. Ivanyuk, and H. Hofmann, Nucl. Phys. A **612** (1997), 1.
[31] F.A. Ivanyuk, H. Hofmann, V.V. Pashkevich and S. Yamaji, Phys. Rev. C **55** (1997), 1730.